THE JOURNAL OF PHYSICAL CHEMISTRY A
A JOURNAL OF THE AMERICAN CHEMICAL SOCIETY

pubs.acs.org/JPCA

Article

Thermochemistry and Kinetics of the Atmospheric Oxidation Reactions of Propanesulfinyl Chloride Initiated by OH Radicals: A Computational Approach

Parandaman Arathala and Rabi A. Musah*

Cite This: J. Phys. Chem. A 2022, 126, 4264−4276

Read Online

ACCESS | Metrics & More | Article Recommendations | Supporting Information

ABSTRACT: The thermochemistry and kinetics of the atmospheric oxidation mechanism for propanesulfinyl chloride ($CH_3-CH_2-CH_2-S(=O)Cl$; PSICl) initiated by the hydroxyl (OH) radical were investigated with high level quantum chemistry calculations and the Master equation solver for multi-energy well reaction (Mesmer) kinetic code. The mechanism for the oxidation of PSICl in the presence of OH radical can proceed via H-abstraction and substitution pathways. The CCSD(T)/aug-cc-pV(T+d)Z//MP2/aug-cc-pV(T+d)Z level calculated energies revealed addition of the OH radical to the S-atom of the sulfinyl (−S(=O)) moiety, followed by cleavage of the Cl−S(=O) single bond, leading to formation of propanesulfinic acid (PSIA) and the Cl radical to be the major pathway when compared to all other possible channels. The transition state barrier height for this reaction was found to be −3.0 kcal mol^{-1} relative to the energy of the starting PSICl + OH radical reactants. The rate coefficients were calculated for all possible paths in the atmospherically relevant temperature range of 200−320 K and at 1 atm. The rate coefficient for the formation of the PSIA + Cl radical from the PSICl + OH radical reaction was found to be 8.2×10^{-12} cm^3 $molecule^{-1}$ s^{-1} at 298 K and a pressure of 1 atm. From branching ratio calculations, it was revealed that the reaction resulting in the formation of the PSIA + Cl radical contributed ∼52% to the total reaction. The overall rate coefficient for the PSICl + OH reaction was also calculated and found to be 1.6×10^{-11} cm^3 $molecule^{-1}$ s^{-1} at 298 K and a pressure of 1 atm. In the aggregate, the results indicate the atmospheric lifetime of PSICl to be ∼12−20 h in the temperature range between 200 and 320 K, which suggests that its contribution to global warming is negligible. However, the degradation products revealed to be formed in its interactions with the OH radical, which include that SO_2, Cl radical, HO_2 radical, and propylene have significant effects on the formation of acid rain, secondary organic aerosols, the ozone layer, and global warming.

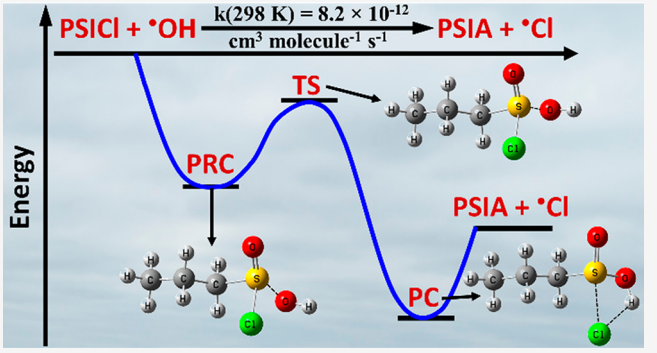

1. INTRODUCTION

Volatile organosulfur compounds (VOSCs) play an important role in atmospheric chemistry and various other areas of science. Hydrogen sulfide (H_2S), carbonyl sulfide (OCS), methanethiol (CH_3SH), dimethyl sulfide ($(CH_3)_2S$), and several other sulfur compounds are ubiquitous in the atmosphere, and their oxidation reactions lead to the production of various low-volatility products. These compounds may have significant effects on global warming, formation of acid rain, and climate change.[1] VOSCs are emitted into the atmosphere from several natural and anthropogenic sources.[2−4] Sulfur compounds are present in various fuels such as heating oil, aircraft fuels, gasoline, and diesel.[5] The most common sulfur compound present in gasoline is thiophene, and other heavy fractions of oil contain benzothiophene and dibenzothiophene.[6] In the atmosphere, sulfur dioxide (SO_2), sulfur trioxide (SO_3), and H_2S are the three principal sulfur-containing pollutants.[7−9] The major sources of SO_2 are fossil fuel consumption, power generation, industrial activities, metal smelting, and petroleum refining.[10,11] H_2S is another important sulfur species that plays a significant role in the atmospheric sulfur cycle. The concentrations of H_2S in volcanic regions and geothermal fields are reported to be about 500 parts per billion (ppb).[12,13] It is emitted from oil and gas producing regions. It has also been reported that H_2S is slowly oxidized to SO_2 by a multistep mechanism that ultimately results in the formation of sulfuric acid (H_2SO_4), which then eventually contributes to the formation of aerosols and acid rain.[9] In addition, removal of sulfur compounds from hydrocarbon sources is used in the synthesis of monomers for mass produced plastics.[14]

Received: February 21, 2022
Revised: May 10, 2022
Published: June 27, 2022

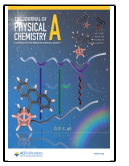

A large number of VOSCs such as thiosulfinates with the general formula R−S(=O)−S−R (where R = $-CH_3$ or $CH_3-(CH_2)_n-$) and other sulfur compounds were detected in the atmosphere of a beech forest with *Allium ursinum* as ground cover.[15] The concentrations of these VOSCs were reported to be in the range of 0.3−7.8 parts per million (ppm), with an average level of 2.9 ppb.[15] The emission of the C_2-C_6 sulfur compounds from *A. ursinum* ranged from ∼44 to ∼100 μg S m^{-2} h^{-1}. The highest mean emission rate for organic sulfur species emitted from a terrestrial plant has been reported to be ∼62 μg S m^{-2} h^{-1}.[15] Dimethyl thiosulfinate (DMTS) and dipropyl thiosulfinate (DPTS) are the most common VOSCs released from various *Allium* genus cash crops[15−18] such as garlic and onions. Therefore, it is important to understand the fate of these compounds and their oxidation products in the presence of important atmospheric oxidants such as hydroxyl (OH) and chlorine (Cl) radicals. Recent computational studies have reported on the oxidation of DMTS and DPTS with OH and Cl radicals.[19−21] Based on these studies, the atmospheric lifetimes of DMTS and DPTS with respect to OH and Cl radicals are very short and their global warming potentials (GWPs) are negligible. However, various products formed from the oxidation of these compounds in the presence of OH and Cl radicals may make significant contributions to global warming, climate alteration, acid rain, and the formation of secondary organic aerosols (SOAs).

A recent computational study reported propanesulfinyl chloride ($CH_3CH_2CH_2S(=O)Cl$, PSICl) as an important trace constituent produced along with the propanethiyl radical (PTR) from the oxidation of plant-derived DPTS with the Cl radical under normal atmospheric conditions.[21] This study found that the reaction resulting in the formation of PSICl + PTR was a major channel, with branching ratios of up to ∼72−74% in the temperatures between 200 and 300 K compared to all other reaction paths associated with the DPTS + $^{\bullet}$Cl reaction. Reactions with the Cl radical are considered to be an important sink for oxidation of atmospheric volatile organic compounds (VOCs). The rate coefficients for the reaction of Cl radical with VOCs are often an order of magnitude larger than the same reactions with the OH radical. Cl radicals are produced in the atmosphere from heterogeneous reaction cycles involving sea salt in the marine boundary layer (MBL). The concentrations of these radicals at the MBL are ∼1−10% those of OH radical levels. In addition, high levels of nitryl chloride ($ClNO_2$), a Cl radical source, have been identified in midcontinental areas such as North America, Central Europe, Western Europe, and northern China.[22−25] Its concentrations were reported to be 1.1 × 10^5 and 1.3 × 10^4 molecules cm^{-3} in areas such as the north China plain and northern Europe, respectively.[26,27] Other sources of Cl radicals in the atmosphere include HCl, HOCl, Cl_2, BrCl, chlorocarbons, and chlorofluorocarbons, and they have various natural and anthropogenic origins. Several studies have also proven that Cl radical reactions can be more important than OH radical reactions for hydrocarbons in regional atmospheres.[27,28] This clearly indicates that Cl radicals also play significant roles in determining the fate of atmospheric organics in coastal urban and continental areas. For this reason, it is important to continue to identify and catalog new sources of Cl radicals.

Terrestrial plant-derived DPTS, when in the presence of Cl radical in continental areas and the MBL, mainly undergoes reactions to form PSICl as a major product.[21] Because Cl radical concentrations can reach 10% of that of OH radicals,[29] this pathway makes a significantly higher contribution to the removal of DPTS in regional atmospheres. Therefore, the PSICl product of the DPTS + Cl radical pathway can be of major significance in regional atmospheres. While the concentration of PSICl has not been measured experimentally in atmospheric ambient air, it has been found to be a key reaction intermediate produced from the oxidation of DPTS.[21] As such, it may contribute to the environmental sulfur burden. Several atmospheric models have been developed for a global sulfur cycle, but all of them underpredict the significant amounts of terrestrial biogenic sulfur required to balance it.[30] This makes the identification of potential sources of atmospheric sulfur critical. In particular, sulfur gas flux from living vascular plants to the environment is an important but little studied part of the global sulfur cycle.[31,32] Therefore, PSICl may be an important biogenic organosulfur compound that contributes to the global sulfur cycle. For this reason, we embarked on a study of its fate in the atmosphere. In addition, however, the study of this molecule may be of relevance to the chemistry of some chemical warfare agents. There is very limited data available on the reactions of chlorinated sulfur hydrocarbons and their S- and Cl-based intermediates in the atmosphere.[5] Bis(2-chloroethyl)sulfide ($(ClCH_2CH_2)_2S$) is a major chemical warfare agent that was manufactured in the early 1910s.[5] Given the relationship between the structure of PSICl to that of bis(2-chloroethyl)-sulfide which also contains S- and Cl-atoms, the study of the oxidative fate of PSICl may provide insights into the chemistry of bis(2-chloroethyl)sulfide that may prove useful in addressing its decomposition and that of similar compounds.

The importance of giving consideration to the degradation mechanism of PSICl under normal atmospheric conditions derives in part from the significant amounts of its precursor (i.e., DPTS) that are released from onion and garlic cash corps and that occupy large acreage on farmlands throughout the world. Thus, PSICl is expected to be formed in the atmosphere from the DPTS + Cl radical reaction. In addition, chlorocarbons are important sources of chlorine radicals in the atmosphere, with photodissociation being a common route to global tropospheric chlorine radical production.[33] These compounds often exhibit relatively long tropospheric lifetimes mainly because of their slow decay in the atmosphere and slow reaction rate with the OH radical.[34] Thus, it was of interest to determine whether PSICl serves as a source of Cl radicals. If it were to diffuse into the stratosphere, then it could disturb the ozone layer.[35] In addition, the presence of sulfur in PSICl may form sulfate particles in the atmosphere, which could be useful in reducing global warming.[36] Sulfur compounds have been proposed as candidates for the geoengineering of a solution to offset climate change in the Earth's atmosphere.[36−38] Therefore, it is important to understand the decomposition mechanism and atmospheric lifetime of PSICl in the presence of the major atmospheric oxidant OH radical, particularly since reactions of OH radicals with many volatile organic compounds are found to be the main sinks in gas phase atmospheric reactions.

In principle, oxidation of PSICl initiated by an atmospheric OH radical could proceed by abstraction and substitution pathways. Specifically, the opportunity for these abstraction and substitution paths occurs because of the presence in PSICl of methylene ($-CH_2$) and methyl ($-CH_3$) groups and the Cl-atom attached to the S-atom of the sulfinyl ($-S(=O)$) moiety, respectively. In addition, the presence of the S-atom within PSICl, provides another substitution path. The possible abstraction and substitution paths are indicated as R1, R2a-b,

https://doi.org/10.1021/acs.jpca.2c01203
J. Phys. Chem. A 2022, 126, 4264−4276

R3a-b, R4a-b, and R5−R6, as shown in Figure 1. The abstraction paths (R1, R2a-b, R3a-b, and R4a-b) in Figure 1 result in the

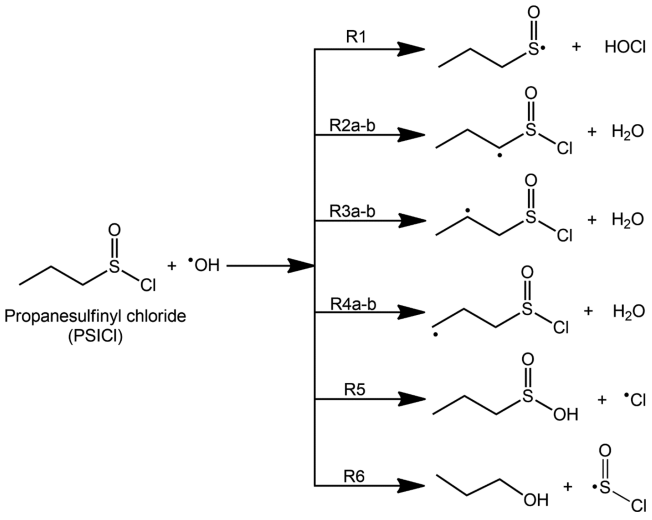

Figure 1. Atmospheric oxidation of propanesulfinyl chloride (PSICl) with the OH radical involving various possible H- and Cl-atom abstraction paths (R1, R2a-b, R3a-b, and R4a-b) to form the corresponding C-centered radical products + H_2O and an S-centered radical product + HOCl, respectively, and substitution paths (R5 and R6) to form the propanesulfinic acid + Cl radical and propanol + SOCl radical, respectively.

formation of S- and various C-centered radicals. Molecular hypochlorous acid (HOCl) accompanies formation of the S-centered radical, and water (H_2O) is formed alongside the C-centered radicals. In the substitution paths (R5 and R6), OH radical addition to the S-atom of the sulfinyl group, followed by Cl−S(=O) single bond fission produces propanesulfinic acid (PSIA) + Cl radical products (R5) while the addition of OH radical to the C-atom of the $-CH_2$ that is directly attached to the sulfinyl group followed by cleavage of the C−S(=O) single bond leads to the formation of propanol ($CH_3CH_2CH_2OH$) and S(=O)Cl radical (R6).

To the best of our knowledge, the atmospheric oxidation mechanism, energetics, and kinetics of the reaction of PSICl with the OH radical have not been reported. Therefore, the complete reaction mechanism, energetics, and kinetics of various possible paths involved in the PSICl + •OH reaction were investigated using high level electronic structure methods. In any molecule + radical reaction in the atmosphere, the formation of the pre-reactive complex (PRC), transition state (TS), post-reactive complex (PC), and products steps is important in understanding the dynamics of the reaction. Thus, all the reaction paths associated with the PSICl + OH radical were characterized by optimizing the corresponding reactants, PRCs, TSs, PCs, and products using both a hybrid density functional method and second-order Møller−Plesset (MP2) perturbation theory. We then calculated energies for all of the stationary points using DFT/*ab initio* electronic structure calculations. These high-level quantum chemistry methods have been successfully used in the investigation of gas phase chemical reactions such as molecule−radical reactions under atmospheric conditions. Thermochemical parameters were calculated to determine the stability of all of the species involved in the various reaction paths. The rate coefficients were calculated for all the reaction paths using the Master equation solver for multi-energy well reactions (Mesmer) kinetic code[39] with Eckart tunneling[40] correction in the atmospherically relevant temperatures between 200 and 320 K and a pressure of 1 atm. Branching ratio calculations were performed to assess the percentage contribution from each reaction path to the overall reaction. The present work is useful in understanding the fate of PSICl in the presence of OH radical under atmospheric conditions, and the atmospheric implications of the results are discussed.

2. COMPUTATIONAL METHODS

All electronic structure calculations in the present work were performed using Gaussian 16 software.[41] The geometry optimization of all of the key stationary points on the potential energy surfaces (PESs) for the various possible reaction paths associated with the PSICl + •OH reaction was performed using both MP2 perturbation theory[42] and M06-2X hybrid density functional methods.[43] M06-2X and MP2 methods have been successfully used in previous studies for determining the reaction mechanism, long-range interactions, energy barriers, thermochemistry, and kinetics with high accuracy for various important reactions involving sulfur and other compounds.[19,44−48] All calculations in this work were performed using the aug-cc-pV(T+d)Z basis set at both levels of theory to get accurate geometries, energies, and vibrational frequencies. This basis set adds tight d functions to the S-atom, which helps to provide a more accurate rendering of the bonding in S-containing species.[49,50] The harmonic vibrational frequency calculations for all the key stationary points were also performed using both levels of theory. Reactants, PRCs, PCs, and products were identified with all positive vibrational frequencies, and the TSs were identified with one imaginary (negative) vibrational frequency. Intrinsic reaction coordinate (IRC)[51] calculations were carried out to ensure that each transition state connected with its corresponding PRC and PC on the reaction coordinate. In addition, single-point energy calculations were performed for all the minima on the PESs to get more accurate energies at cost-effective coupled-cluster single, double, and triple excitation (CCSD(T)) methods using the same aug-cc-pV(T+d)Z basis set on the previously optimized geometries at the M06-2X/aug-cc-pV(T+d)Z and MP2/aug-cc-pV(T+d)Z levels. This higher level CCSD(T) method is known to provide benchmark quality binding energies for noncovalently bound systems.[52−54] Furthermore, using this approach, errors of relative energies and bond energies can often be calculated to within 1 kcal mol^{-1}.[55] The zero-point energies (ZPEs) computed at the M06-2X/aug-cc-pV(T+d)Z and MP2/aug-cc-pV(T+d)Z levels were used to correct the corresponding single-point energies for all the stationary points calculated at the CCSD(T)/aug-cc-pV(T+d)Z level. In addition, T1 diagnostic calculations were performed to assess whether the observed results for the single reference-based CCSD(T) wavefunction were reliable. In general, stationary points having T1 values larger than 0.02 are considered to be less reliable and require the further application of a multireference-based electron correlation procedure.[56] In the present work, T1 values calculated at the CCSD(T)/aug-cc-pV(T+d)Z level for all the species are provided in Table S1 of the Supporting Information. The results suggest that, for all of the species, T1 values are ≤0.02 except for that associated with transition state (TS6), whose T1 value was found to be ∼0.03 (see Table S1). Thus, the single reference-based CCSD(T) wavefunction was found to be appropriate in the present work. The calculated total electronic energies (E_{total}) and corresponding zero-point energy (ZPE) corrected electronic energies

https://doi.org/10.1021/acs.jpca.2c01203
J. Phys. Chem. A 2022, 126, 4264−4276

[E_{total}(ZPE)] at various levels of theory are given in Tables S2 and S3. In addition, imaginary frequencies for all the possible TSs, rotational constants, vibrational frequencies, and the optimized geometries of all the stationary points at both the M06-2X and MP2 levels are provided in Tables S4−S8 in the Supporting Information.

3. RESULTS AND DISCUSSION

The study of the atmospheric removal process for PSICl in the presence of OH radical was investigated by first determining its most stable conformer. Accordingly, conformational analysis of PSICl was performed by rotating its two adjacent C−C and one C−S single bonds through their corresponding dihedral angles. This process leads to various stable conformers, all of which were optimized at both the M06-2X/aug-cc-pV(T+d)Z and MP2/aug-cc-pV(T+d)Z levels. The more stable geometries observed at the MP2/aug-cc-pV(T+d)Z and M06-2X/aug-cc-pV(T+d)Z levels are shown in Figure 2 and Figure S1 of the Supporting Information, respectively. The relative energies of the most stable conformers were estimated at both the M06-2X and MP2 levels using the same aug-cc-pV(T+d)Z basis set and are provided in Table S9 of the Supporting Information. The results from Table S9, Figure 2, and Figure S1 indicate that structure PSICl-III is the most stable conformer. The relative energies observed in the present calculations at both the M06-2X and MP2 levels indicate that structures PSICl-I, PSICl-II, and PSICl-IV are ∼0.2, ∼1.0, and ∼0.5 kcal mol^{-1} higher in energy than structure PSICl-III, respectively. Therefore, the most stable conformer of propanesulfinyl chloride (i.e., structure PSICl-III) was used in the present calculations to investigate its atmospheric removal mechanism in the presence of OH radical.

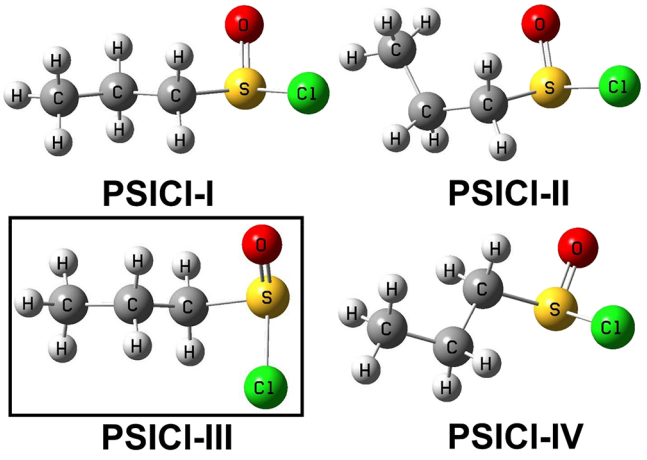

Figure 2. Stable conformations of propanesulfinyl chloride (PSICl) optimized at the MP2/aug-cc-pV(T+d)Z level. The black, white, yellow, red, and green colors represent carbon, hydrogen, sulfur, oxygen, and chlorine atoms, respectively. The PSICl-III shown in the black box is ∼0.2, ∼1.0, and ∼0.5 kcal mol^{-1} more stable than structures PSICl-I, PSICl-II, and PSICl-IV, respectively, as indicated by the energies listed in Table S9.

3.1. Stationary Points on the Potential Energy Surfaces and Energetics. The molecular structure of PSICl contains a propyl moiety and a Cl-atom directly attached to the S-atom of the sulfinyl (S(=O)) group. Its interaction with the atmospheric OH radical is expected to occur primarily through H-atom abstraction and substitution pathways, as delineated in Figure 1. The abstraction by the OH radical of H- and Cl-atoms linked to the C-atoms of the propyl and S(=O) groups of PSICl, respectively, was investigated. In Figure 3, the transition state for abstraction of the Cl-atom from PSICl is labeled as TS1. As the four H-atoms contained within the two −CH_2 groups in PSICl are all different from one other, four TSs labeled TS2a, TS2b, TS3a, and TS3b emerge. With reference to the −CH_3 moiety of PSICl, the M06-2X/aug-cc-pV(T+d)Z and MP2/aug-cc-pV(T+d)Z level calculations indicated that two of the H-atoms are the same and distinguished from the third. Thus, the results suggest only two different TSs for abstractions involving the −CH_3 group, and these are labeled as TS4a and TS4b in Figure 3. Therefore, overall, there are a total of six different H-abstraction TSs and one Cl-abstraction TS that are possible for the PSICl + OH radical reaction. These are all labeled as shown in Figure 3.

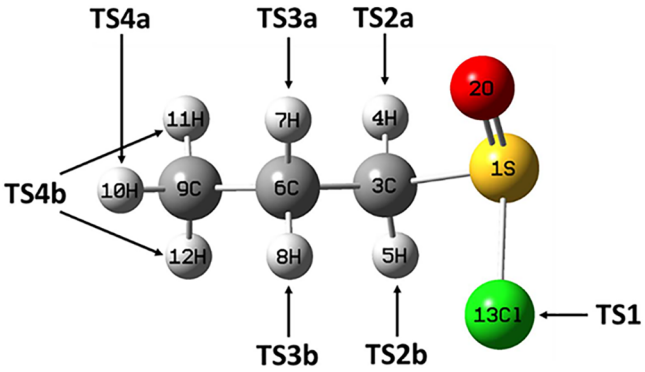

Figure 3. Labeling of the seven possible distinct Cl- and H-atom abstractions from the propanesulfinyl chloride by the OH radical, leading to transition states. The symbols are defined as follows: TS1: transition state for Cl-atom abstraction; TS2a, TS2b, TS3a, TS3b, TS4a, and TS4b: transition states for H-atom abstraction.

The abstraction pathways (R1−R4a-b) given in Figure 1 lead to the formation of C- and S-centered radical products. The products formed from reaction pathway R1 are labeled P_1 ($(CH_3CH_2CH_2S^{\bullet}(=O))$ + hypochlorous acid (HOCl)). The products formed from the abstraction pathways R2a-b, R3a-b, and R4a-b are labeled P_2 (CH_3-CH_2-$C^{\bullet}H$−S(=O)Cl) + water (H_2O), P_3 (CH_3−$C^{\bullet}H$−CH_2-S(=O)Cl) + H_2O, and P_4 ($C^{\bullet}H_2$−CH_2−CH_2−S(=O)Cl) + H_2O, respectively (see Figure 1).

Similarly, substitution pathways (R5 and R6) are also possible for the PSICl + OH radical reaction (see Figure 1). The transition state and corresponding products for the addition of OH radical to the S-atom of the sulfinyl moiety, followed by S(=O)−Cl single bond cleavage, leading to PSIA and Cl radical through substitution channel R5 are labeled TS5, P_5, and $^{\bullet}$Cl, respectively. The remaining transition state and products formed from OH addition to the C-atom of the −CH_2 moiety, followed by C−S(=O) single bond cleavage, leading to the formation of propanol and the S(*O*)Cl radical through substitution channel (R6) are labeled TS6, P_6, and SOCl, respectively.

The relative energies of all the key stationary points present on all PES profiles associated with the PSICl + OH radical reaction obtained at both the CCSD(T)/aug-cc-pV(T+d)Z//M06-2X/aug-cc-pV(T+d)Z (designated as CCSD(T)//M06-2X) and CCSD(T)/aug-cc-pV(T+d)Z//MP2/aug-cc-pV(T+d)Z (designated as CCSD(T)//MP2) levels are given in Table 1. The results from Table 1 indicate that the relative energies at both

https://doi.org/10.1021/acs.jpca.2c01203
J. Phys. Chem. A 2022, 126, 4264−4276

Table 1. Zero-Point Energy (ZPE) Corrected Energies, Enthalpies, and Free Energy Changes Calculated for the Various Paths Associated with the Propanesulfinyl Chloride (PSICl) + OH Radical Reaction at Various Levels of Theory[a]

		CCSD(T)/aug-cc-pV(T+d)Z//MP2/aug-cc-pV(T+d)Z			CCSD(T)/aug-cc-pV(T+d)Z//M06-2X/aug-cc-pV(T+d)Z		
pathway	stationary point	$\Delta(E+\mathrm{ZPE})$[b]	$\Delta H(298\ \mathrm{K})$[b]	$\Delta G(298\ \mathrm{K})$[b]	$\Delta(E+\mathrm{ZPE})$[c]	$\Delta H(298\ \mathrm{K})$[c]	$\Delta G(298\ \mathrm{K})$[c]
R1	PSICl + $^{\bullet}$OH	0.0	0.0	0.0	0.0	0.0	0.0
	PRC1	−4.9	−5.2	2.0	−4.6	−5.0	3.1
	TS1	10.4	9.7	2.0	8.1	7.6	15.9
	PC1	−7.0	−7.4	−0.3	−7.0	−7.4	−0.2
	P_1 + HOCl	1.4	1.0	−1.4	0.8	0.4	−2.0
R2a	PRC2	−5.2	−5.6	2.2	−5.0	−5.5	3.0
	TS2a	0.5	−0.3	8.9	0.5	−0.3	9.0
	PC2	−24.6	−24.4	−18.2	−24.4	−24.2	−17.3
	P_2 + H_2O	−19.4	−19.0	−21.4	−19.8	−19.2	−22.6
R2b	PRC3	−3.1	−3.2	4.0	−3.0	−3.1	4.0
	TS2b	0.9	0.1	9.2	0.8	0.1	9.1
	PC3	−23.9	−23.6	−17.3	−24.2	−23.8	−17.4
R3a	TS3a	−1.6	−2.5	7.0	−1.5	−2.4	7.0
	PC4	−26.1	−25.9	−19.1	−26.0	−25.8	−18.9
	P_3 + H_2O	−20.7	−20.2	−22.2	−20.7	−20.2	−22.3
R3b	TS3b	0.4	−0.3	8.5	0.7	0.0	8.8
	PC5	−24.2	−23.7	−17.5	−24.2	−23.6	−17.7
R4a	TS4a	2.6	2.1	9.3	2.8	2.2	9.9
	PC6	−20.2	−19.6	−13.5	−17.4	−16.7	−12.1
	P_4 + H_2O	−16.4	−15.8	−17.9	−16.3	−15.7	−18.0
R4b	TS4b	1.5	0.9	9.1	1.8	1.0	9.5
	PC7	−20.2	−19.6	−13.5	−18.9	−18.4	−11.8
R5	PRC4	−4.1	−2.9	3.1			
	TS5	−3.0	−4.7	3.6			
	PC8	−27.3	−28.4	−18.5			
	P_5 + $^{\bullet}$Cl	−13.2	−13.8	−11.9			
R6	TS6	18.1	17.4	26.4	17.6	16.9	25.7
	PC9	−39.2	−39.2	−33.6	−38.9	−38.9	−33.3
	P_6 + SOCl	−36.4	−37.1	−39.5	−36.9	−37.6	−40.0

[a]All values are in kcal mol^{-1}. [b]Values computed at the CCSD(T)/aug-cc-pV(T+d)Z//MP2/aug-cc-pV(T+d)Z level with zero-point corrections, enthalpy, and free energy corrections obtained at the MP2/aug-cc-pV(T+d)Z level. [c]Values computed at the CCSD(T)/aug-cc-pV(T+d)Z//M06-2X/aug-cc-pV(T+d)Z level with zero-point corrections, enthalpy, and free energy corrections obtained at the M06-2X/aug-cc-pV(T+d)Z level.

the CCSD(T)//M06-2X and CCSD(T)//MP2 levels for PRCs, TSs, PCs, and products exhibit maximum deviations of ∼0.3, ∼0.5, ∼2.5, and ∼0.6 kcal mol^{-1}, respectively. This suggests that the relative energies obtained at both levels of theory were in reasonably good agreement with one another (see Table 1). We also noted that the transition state for the substitution channel (R5) in Figure 1 was not identified at the M06-2X and B3LYP levels when the 6-31+G(d,p), 6-311++G(2d,2p), aug-cc-pVTZ, and aug-cc-pV(T+d)Z basis sets were used. However, we identified this important transition state at the MP2/aug-cc-pV(T+d)Z level. Therefore, the results obtained at the CCSD(T)//MP2 level were used for the energies and in the rate coefficient calculations to facilitate direct comparison with other possible pathways involved in the PSICl + OH radical reaction.

3.1.1. Abstraction Paths. We now present our results for the abstraction paths (R1−R4a-b) associated with the PSICl + OH radical reaction (see Figure 1). The potential energy profiles containing all the key stable minima such as reactants, PRCs, TSs, PCs, and products for all possible H- and Cl-abstraction pathways are labeled R1−R4a-b and are shown in Figure 4. The energies of all the stationary points calculated at the CCSD(T)/aug-cc-pV(T+d)Z//MP2/aug-cc-pV(T+d)Z level are also displayed in Figure 4, and all of the values are calculated relative to the energy of the starting PSICl + $^{\bullet}$OH reactants. Table 1 contains relative energies, enthalpies, and free energies calculated at 298 K for all the key stationary points present on all possible PESs associated with the PSICl + OH radical system. The optimized geometries of all the minima obtained at the MP2/aug-cc-pV(T+d)Z level are shown in Figure 5. The important bond lengths (Å), bond angles, and hydrogen bonding interactions are shown for all the structures (see Figure 5). All of the possible H- and Cl-atom abstraction paths initially proceed through the formation of stable van der Waals complexes (PRCs) such as PRC1, PRC2, and PRC3 from the association of two reactants through hydrogen bonding interactions. The hydrogen bonding interaction in PRC1 is mainly between the O-atom of the OH radical and the H-atom of the center methylene moiety of PSICl, with a bond length of 2.61 Å, and bonding between the H-atom of the OH radical and O-atom of PSICl with a bond length of ∼1.92 Å (see Figure 5). In PRC2, hydrogen bonding occurs between the O-atom of the OH radical and the two H-atoms of the propyl moiety of PSICl, with bond lengths of 2.65 and 2.81 Å, respectively. Hydrogen bonding is also observed between the H-atom of the OH radical and the O-atom of PSICl, with a bond length of ∼1.94 Å. Similarly, hydrogen bonding interactions were also seen in PRC3, with bonding between the O-atom of the OH radical and the H-atoms of the $-CH_2-CH_3$ moiety of PSICl with bond lengths of 2.87 and 2.88 Å, respectively, and bonding between

https://doi.org/10.1021/acs.jpca.2c01203
J. Phys. Chem. A 2022, 126, 4264−4276

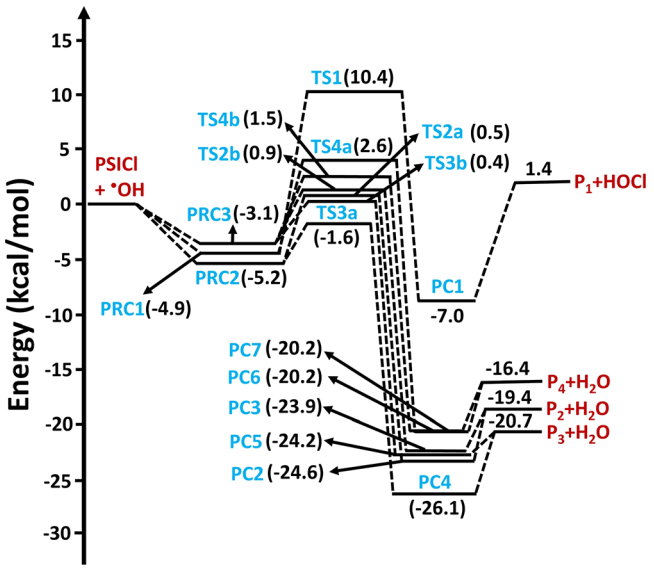

Figure 4. Potential energy profiles for all possible abstraction paths associated with the PSICl + •OH reaction obtained at the CCSD(T)/aug-cc-pV(T+d)Z//MP2/aug-cc-pV(T+d)Z level. The symbols are defined as follows: PRC1−PRC3 (pre-reactive complexes); TS1, TS2a, TS2b, TS3a, TS3b, TS4a, and TS4b (transition states); PC1−PC7 (post-reactive complexes); and P_1−P_4 (S-atom and C-atom centered radical products).

the H-atom of the OH radical and Cl-atom of PSICl with a bond length of ∼2.44 Å. The binding energies of PRC1, PRC2, and PRC3 were estimated to be 4.9, 5.2, and 3.1 kcal mol^{-1}, respectively, below those of the starting reactants. This can be clearly seen at the entrance channels of each reaction path (see Figure 4). The reason for the greater stability of these complexes is mainly due to the presence of hydrogen bonding interactions. The reaction then proceeds from PRC1 to form two transition states (TS1 and TS4a) with barrier heights of 10.4 and 2.6 kcal mol^{-1}, respectively. The optimized structures for PRC1 and TS1 in Figure 5 show that the rotation of the OH group in PRC1 occurs in such a way that it abstracts the Cl atom of PSICl. The structures of PRC1 and TS4a indicate that the O-atom of the OH radical from PRC1 abstracts the H-atom of the methyl group as shown in TS4a (see Figure 5). These two reaction TSs further proceed to form their corresponding post-reactive complexes (PC1 and PC6) on the PESs with energies of −7.0 and −20.2 kcal mol^{-1}, respectively. PC1 and PC6 then undergo decomposition to form final products [P_1 ($CH_3CH_2CH_2S^{\bullet}$(=O)) + HOCl] and [P_4 ($^{\bullet}CH_2CH_2CH_2S$(=O)Cl) + H_2O], which are located on the PES with corresponding energies of 1.4 and −16.4 kcal mol^{-1}, respectively. The formed second pre-reactive complex (PRC2) leads to the formation of two transition states (TS2a and TS3a) with corresponding barrier heights of 0.5 and −1.6 kcal mol^{-1} above and below that of the starting reactants, respectively. These two TSs further proceed to form their corresponding post-reactive complexes (PC2 and PC4) with energies of −24.6 and −26.1 kcal mol^{-1}, respectively. The formed PCs then lead to the formation of [P_2 ($CH_3CH_2C^{\bullet}HS$(=O)Cl) + H_2O] and [P_3 ($CH_3C^{\bullet}HCH_2S$-(=O)Cl) + H_2O] bimolecular products at −19.4 and −20.7 kcal mol^{-1}, respectively. The remaining pre-reactive complex (PRC3) proceeds to form three different transition states (TS2b, TS3b, and TS4b) with corresponding barrier heights of 0.9, 0.4, and 1.5 kcal mol^{-1}, respectively, which are located above the starting reactants. The formed TSs are connected with the corresponding PC3, PC5, and PC7, with energies of −23.9, −24.2, and −20.2 kcal mol^{-1}, respectively. The reaction paths further lead to the formation of the final products [P_2 ($CH_3CH_2C^{\bullet}HS$(=O)Cl) + H_2O], [P_3 ($CH_3C^{\bullet}HCH_2S$(=O)Cl) + H_2O], and [P_4 ($^{\bullet}CH_2CH_2CH_2S$(=O)Cl) + H_2O] with corresponding energies of −19.4, −20.7, and −16.4 kcal mol^{-1}, respectively. Based on the energies of all the transition states provided in Figure 4, abstraction of the H-atom via TS3a has the lowest barrier and is the most dominant compared to all the possible H- and Cl-atom abstraction paths involved in the PSICl + •OH reaction.

3.1.2. Substitution Paths. We now present the energetics of the possible substitution channels associated with the PSICl + OH radical reaction. The potential energy profiles involving important stationary points obtained at the CCSD(T)/aug-cc-pV(T+d)Z//MP2/aug-cc-pV(T+d)Z level are shown in Figure 6. The energy values for all the stationary points displayed in Figure 6 were estimated relative to the energy of the starting reactants. The PES profiles for the substitution channels R5 and R6 (see Figure 1) proceed similar to the abstraction path described above. The results in Figure 6 suggest that the association of PSICl and the OH radical initially forms a stable pre-reactive complex (PRC4) with a binding energy of ∼4.1 kcal mol^{-1} below that of the starting reactants. The stability of this complex is due to the formation of a two-center−three-electron (2c-3e) bond between the lone pair electrons of the S-atom of PSICl and the single-electron occupied p-orbital of the OH radical. Similar 2c-3e bonded complexes have been reported in previous studies of OH··DMS and OH··DMSO reactions.[57−59] PRC4 then proceeds further to produce stable PC8 with an energy of −27.3 kcal mol^{-1} through TS5, with a barrier height of −3.0 kcal mol^{-1} below the energy of the starting reactants. The structure of TS5 shown in Figure 5 indicates that the addition of the OH radical to the S-atom of the sulfinyl (−S(=O)) moiety to form a new single bond is followed by cleavage of the Cl−S(=O) single bond. The bond formation and bond cleavage are illustrated with dotted lines in the transition state structure (TS5) (see Figure 5). The reaction then continues to form propanesulfinic acid (P_5) + Cl radical products with an energy of −13.2 kcal mol^{-1}. The negative barrier height for this reaction indicates that this pathway is accessible at normal atmospheric temperatures and pressures. We also calculated the energies for all the key stationary points on the PES involving the substitution channel (R6) to form propanol (P_6) + S(*O*)Cl radical products at the CCSD(T)//MP2 level (see Figures 1 and 6). Similar to the other reaction paths, the PSICl + OH radical results in PRC1, which then leads to transition state (TS6) with a barrier height of 18.1 kcal mol^{-1} above that of the starting reactants. The structure of TS6 in Figure 5 clearly suggests that the O-atom of the OH radical attacks the C-atom of the methylene moiety, which is attached directly to the sulfinyl group of PSICl, by forming a new C−O single bond followed by the cleavage of the C−S(=O) single bond. The reaction then continues to form PC9 at −39.2 kcal mol^{-1}, which then undergoes dissociation to produce propanol (P_6) + S(*O*)Cl radical bimolecular products at −36.4 kcal mol^{-1} (see Figure 6). The higher barrier for this reaction suggests that it may occur only under high-temperature conditions. Overall, based on the energetics of all of the possible reaction paths discussed above, it is the formation of propanesulfinic acid (P_5) + Cl radical products from the substitution channel that proceeds through TS5 that is most dominant when compared to the other possible

https://doi.org/10.1021/acs.jpca.2c01203
J. Phys. Chem. A 2022, 126, 4264−4276

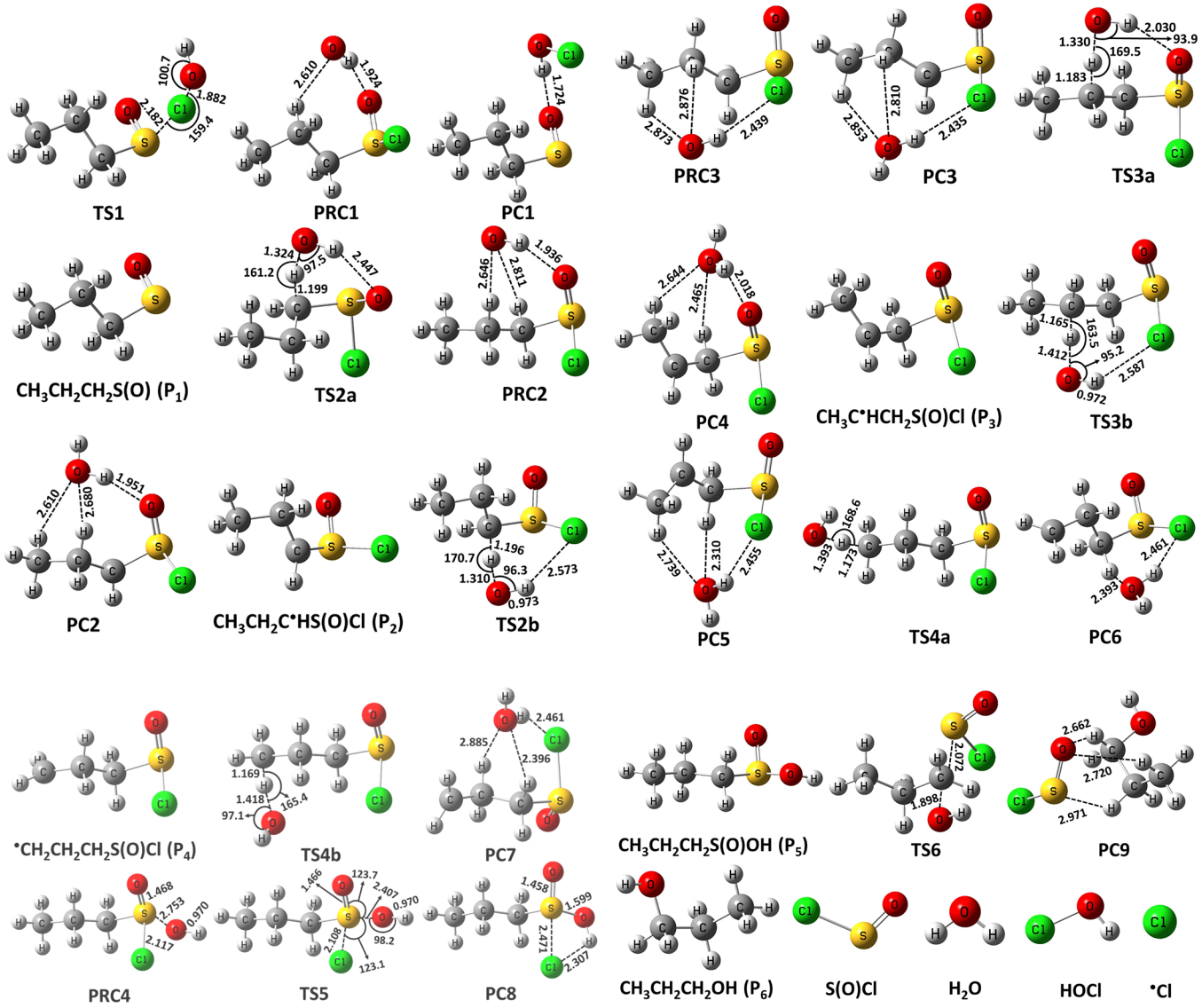

Figure 5. MP2/aug-cc-pV(T+d)Z level-optimized geometries of the pre-reactive complexes (PRCs), transition states (TSs), product complexes (PCs), and products for all possible reaction paths involved in the propanesulfinyl chloride + OH radical reaction. The black, yellow, white, green, and red colors represent carbon, sulfur, hydrogen, chlorine, and oxygen atoms, respectively. The bond lengths (in Å) calculated at the MP2/aug-cc-pV(T+d)Z level are shown.

abstraction and substitution paths available to the PSICl + OH radical system.

Thermodynamic parameters such as enthalpy (ΔH) and Gibbs free energy (ΔG) at 298 K for all of the minima on the PESs associated with all possible abstraction and substitution pathways were calculated at the CCSD(T)//M06-2X and CCSD(T)//MP2 levels. Table 1 displays the computed values for all of the stationary points relative to the starting reactants. The values of enthalpy and Gibbs free energy changes for all the stationary points at both levels agree reasonably well with each other (see Table 1). The results from Table 1 suggest that the reaction free energies for the abstraction of the H-atom through R2a, R2b, R3a, R3b, R4a, and R4b are more spontaneous than those for the abstraction of the Cl-atom from PSICl that proceeds through R1. The changes in Gibbs free energy (ΔG) for these reactions through R2a, R2b, R3a, R3b, R4a, and R4b were found to be −21.4, −21.4, −22.2, −22.2, −17.9, and −17.9 kcal mol^{-1}, respectively, computed at the CCSD(T)//MP2 level. The change in enthalpy (ΔH) for the H-atom abstraction channels associated with the PSICl + OH radical reaction that proceeds through R2a, R2b, R3a, R3b, R4a, and R4b was found to be more exothermic than the abstraction of the Cl-atom from PSICl through R1. This clearly suggests that the abstraction of the H-atom from the C-atom of the propyl moiety of PSICl is more exothermic and highly favored than the Cl-atom abstraction associated with the PSICl + OH radical reaction. The reaction enthalpies for the substitution channels via R5 and R6 were found to be −13.8 and −37.1 kcal mol^{-1}, respectively. The free energies for the same reactions were found to be −11.9 and −39.5 kcal mol^{-1}, respectively, which suggests that these reaction paths are exothermic and spontaneous in nature.

4. THEORETICAL KINETIC ANALYSIS

Master equation solver for multi-energy well reactions (Mesmer v.5.2) software[39] was used to calculate the rate coefficients for all possible abstraction and substitution paths investigated in the present work. Several previously reported studies have used this code in determining the rate coefficients for various atmospheri-

https://doi.org/10.1021/acs.jpca.2c01203
J. Phys. Chem. A 2022, 126, 4264−4276

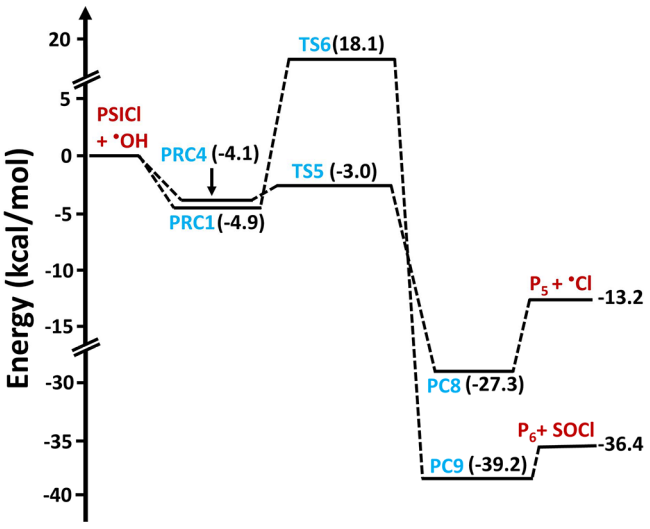

Figure 6. Potential energy surface diagram for the substitution channels involved in the propanesulfinyl chloride + OH radical reaction leading to various products, computed at the CCSD(T)/agu-cc-pV(T+d)Z//MP2/aug-cc-pV(T+d)Z level. The symbols are defined as follows: PRC1 and PRC4 (pre-reactive complexes); TS5 and TS6 (transition states); PC8 and PC9 (post-reactive complexes); and P_5 and P_6 (products).

cally important reactions[60−62] as well as reactions of sulfur compounds with OH radicals.[19,20] A detailed description of Mesmer is given in our previous work[19] and studies from other groups.[39,60,63] Mesmer solves the Master equation to provide phenomenological rate coefficients for the system using the subsequent eigenvalue−eigenvector analysis.[64] The zero-point energy (ZPE) corrected CCSD(T) energies of all the species shown on the PESs were obtained from the quantum chemical calculations conducted in this work, and these values were used for the kinetic modeling.

The PES profiles observed here indicate that the association of PSICl and OH radical reactants in all possible abstraction and substitution paths primarily form barrierless hydrogen bonded PRCs. No definitive transition state structures were located for the association of PSICl and the OH radical to form the corresponding pre-reactive complexes (such as PRC1, PRC2, PRC3, and PRC4). Therefore, these entrance channels may be barrierless. This was confirmed through a relaxed scan by decreasing the bond lengths between the O-atom of the OH radical and the H-atom or S-atom of PSICl in the starting reactants leading to the formation of their corresponding PRCs. The calculations indicated that the potential energy decreased on the reaction coordinate until the formation of the corresponding PRCs from their initial reactants. This suggests that the entrance channels are barrierless. The PRCs then lead to post-reactive complexes (PCs) via their corresponding transition states (TSs). The formed PCs then undergo decomposition to produce the corresponding final products. The calculation of rate coefficients for barrierless reaction steps is always difficult, and it requires advanced methods such as variational transition state theory (VTST) to find the dividing position between reactants and PRCs that minimize the dissociation rate coefficient. This is because the location of the transition state is not fixed, and it varies along the reaction coordinate as a function of energy. Mesmer handles the barrierless reaction steps shown at the entrance and exit channels of all the reaction paths on the PES (see Figures 4 and 6) using the inverse Laplace transform (ILT) approach to obtain the microcanonical rate coefficients ($k(E)$). For barrierless association reactions, Mesmer uses the ILT approach to calculate microcanonical rate coefficients. The expression that Mesmer transforms is the modified Arrhenius equation $k_\infty(T) = A\left(\frac{T}{T_0}\right)^n e^{-E_a/RT}$. In this expression, $k_\infty(T)$ is the rate coefficient at the high pressure limit, A represents the pre-exponential factor, T is the reaction temperature, T_0 is the reference temperature, n is the modified Arrhenius parameter, and E_a is the activation energy. In the present calculations, T_0 was defined as 298 K. The Arrhenius pre-exponential factor (A) used for the present rate calculations was 1.0×10^{-11} cm^3 molecule^{-1} s^{-1} for the entrance and exit channels of the abstraction and substitution paths. The calculations using this value provided rate coefficients for the PSICl + OH radical reaction, which agreed well with experimentally measured rate coefficients for reactions of similar compounds with the OH radical.[65] In addition, rate coefficients were also monitored as a function of variations in A by up to 2 orders of magnitude. We observed that the rate coefficients changed by ∼2−3 times in the studied temperature range. The association reaction steps were found to be barrierless, and therefore, the activation energy (E_a) is small; it was assumed to be 0 kcal mol^{-1} in the ILT calculations. The temperature dependence for all possible reaction paths associated with the PSICl + OH radical reaction was determined using the modified Arrhenius parameter (n). E_a and n were set to 0 kcal mol^{-1} and 0.1, respectively, in the present calculations. The results using these values and the ground level atmospheric OH radical concentration suggest that the association of the OH radical and PSICl to form the corresponding PRCs occurs on the time scale of some tens of nanoseconds. The rate coefficients for the reactions associated with the conversion of PRCs to PCs through tight transition states were calculated using Rice−Ramsperger−Kassel−Marcus (RRKM) theory. In addition, the Eckart tunneling[40] approach was used to account for the tunneling contributions for all the reaction paths in the studied temperature range.

The single-exponential down model (ΔE_{down}) was used in the Mesmer rate calculations to account for the collision energy transfer between the nitrogen (N_2) bath gas and the modeled species involving all possible reaction paths. The energy transfer parameter in the single exponential down model for all the reaction paths was set to $\langle \Delta E_d \rangle = 200$ cm^{-1}. We used this value based on analogous atmospheric reactions with OH radicals that have been reported in the literature.[44,66] In addition, Mesmer rate calculations require Lennard-Jones (L-J) parameters (ε and σ). The depth of the potential well (ε) and the finite length where the potential is zero (σ) for the PRCs and PCs involved in all the abstraction and substitution paths and the buffer gas were taken from previous reports. Specifically, L-J parameters of σ = 3.9 Å and ε = 48 K[39] were used for the nitrogen buffer. The PRCs and PCs were assumed to have the same L-J parameter values as n-heptane, with σ = 4.42 Å and ε = 306.5 K.[67] These values were used because of the similarity of the size of all the adducts present in the PSICl + OH radical reactions with that of n-heptane. It should be noted that we also considered the L-J parameters for n-hexane and n-octane (in comparison to n-heptane) for the PRCs and PCs but found that the variations in the rate coefficients for all reaction paths were insignificant (hence the use of n-heptane).

4.1. Rate Coefficients. All of the above-mentioned parameters such as vibrational frequencies, rotational constants,

https://doi.org/10.1021/acs.jpca.2c01203
J. Phys. Chem. A 2022, 126, 4264−4276

zero-point corrected energies, the Arrhenius pre-exponential factor, activation energies, the modified Arrhenius parameter, the collision energy transfer, and L-J parameters are required as inputs in the Mesmer code for the determination of temperature-dependent rate coefficients for all the possible reaction paths involved in the PSICl + OH radical reaction. The bimolecular rate coefficients (in cm^3 $molecule^{-1}$ s^{-1}) given in Table 2 for all reaction paths were calculated in the temperatures between 200 and 320 K and at 1 atm pressure. The data in Table 2 indicate that the abstraction of the H-atom from the middle C-atom of the propyl group of PSICl that proceeds through the transition state (TS3a) is a major channel compared to all of the other possible abstraction paths. For example, the rate coefficient for this reaction path at 298 K and 1 atm pressure was estimated to be 4.3×10^{-12} cm^3 $molecule^{-1}$ s^{-1}, which is 1−8 orders of magnitude larger than those for all the other abstraction channels.

We also calculated the bimolecular rate coefficients for the two possible substitution channels in the same studied temperature range. The obtained rate coefficient values are also displayed in Table 2. The rate coefficient value for the substitution reaction via TS5 is 8.2×10^{-12} cm^3 $molecule^{-1}$ s^{-1} at 298 K, which is $\sim 10^{14}$ times larger than the value of the substitution reaction via TS6 with a value of 4.6×10^{-26} cm^3 $molecule^{-1}$ s^{-1} at the same temperature. By comparing the rate coefficients of all possible abstraction and substitution channels associated with the PSICl + OH radical reaction, it is apparent that the reaction that proceeds through TS5 to form PSIA + Cl radical products is kinetically more dominant. This is because the rate coefficient value at 298 K for this reaction is ∼2 times larger than that for the second fastest reaction that occurs via TS3a (see Table 2). Overall, the energetics and kinetics results indicate that the interaction of PSICl with the OH radical mainly proceeds to form PSIA and the Cl radical under normal atmospherically relevant conditions.

In addition, the overall rate coefficients for the oxidation of the PSICl + OH radical under atmospherically relevant conditions were calculated by adding all possible abstraction and substitution path rate coefficients at each temperature. The obtained overall rate coefficient values are given in Table 2 and are plotted in Figure 7 in the temperature range of 200−320 K and at 1 atm. The results in Table 2 and Figure 7 indicate that the overall reaction rate coefficients decrease gradually as the temperature increases from 200 to 320 K. For example, the calculated overall rate coefficients for the PSICl + OH radical reaction at 200 and 320 K were estimated to be 2.3×10^{-11} and 1.5×10^{-11} cm^3 $molecule^{-1}$ s^{-1}, respectively. The present overall rate coefficient values for the PSICl + OH radical reaction were also compared with the values for the PSIA + OH radical reaction in the same range of temperatures and under identical pressure conditions (as shown in Figure 7). From the results shown in Figure 7, it is concluded that the overall rate coefficients for both the PSICl + OH and PSIA + OH radical reactions show similar trends in the studied temperature range. The results also indicate that the overall rate coefficients for the PSICl + OH radical reaction are ∼5−6 times smaller than the values reported for the PSIA + OH radical reaction. For example, the overall rate coefficient calculated for the PSICl + OH radical reaction at 298 K was ∼5 times smaller than that for the PSIA + OH radical reaction, which was reported to be $\sim 8.4 \times 10^{-11}$ cm^3 $molecule^{-1}$ s^{-1} at the same temperature. The reason for the larger rate coefficients for the PSIA + OH radical reaction as compared to the values for the PSICl + OH radical reaction is

Table 2. Bimolecular Rate Coefficients (in cm^3 $molecule^{-1}$ s^{-1}) for Various Possible Reaction Paths Associated with the Reaction of Propanesulfinyl Chloride with OH Radical Calculated in the Temperatures between 200 and 320 K and a Pressure of 1 atm

T	k_{TS1}	k_{TS2a}	k_{TS2b}	k_{TS3a}	k_{TS3b}	k_{TS4a}	k_{TS4b}	k_{TS5}	k_{TS6}	k_{total}[a]
200	3.66×10^{-24}	2.16×10^{-12}	1.55×10^{-12}	7.06×10^{-12}	2.14×10^{-12}	7.42×10^{-13}	4.75×10^{-14}	9.43×10^{-12}	2.94×10^{-31}	2.31×10^{-11}
220	3.10×10^{-23}	1.78×10^{-12}	1.25×10^{-12}	6.39×10^{-12}	1.80×10^{-12}	6.64×10^{-13}	5.21×10^{-14}	9.16×10^{-12}	4.66×10^{-30}	2.11×10^{-11}
240	1.93×10^{-22}	1.48×10^{-12}	1.03×10^{-12}	5.76×10^{-12}	1.54×10^{-12}	6.04×10^{-13}	5.81×10^{-14}	8.90×10^{-12}	6.88×10^{-29}	1.94×10^{-11}
250	4.38×10^{-22}	1.37×10^{-12}	9.50×10^{-13}	5.46×10^{-12}	1.44×10^{-12}	5.81×10^{-13}	6.16×10^{-14}	8.76×10^{-12}	2.44×10^{-28}	1.86×10^{-11}
260	9.40×10^{-22}	1.26×10^{-12}	8.77×10^{-13}	5.19×10^{-12}	1.35×10^{-12}	5.63×10^{-13}	6.55×10^{-14}	8.63×10^{-12}	8.16×10^{-28}	1.79×10^{-11}
280	3.73×10^{-21}	1.10×10^{-12}	7.58×10^{-13}	4.67×10^{-12}	1.20×10^{-12}	5.40×10^{-13}	7.41×10^{-14}	8.38×10^{-12}	7.53×10^{-27}	1.67×10^{-11}
298	1.12×10^{-20}	9.78×10^{-13}	6.76×10^{-13}	4.26×10^{-12}	1.09×10^{-12}	5.31×10^{-13}	8.28×10^{-14}	8.16×10^{-12}	4.55×10^{-26}	1.58×10^{-11}
300	1.26×10^{-20}	9.67×10^{-13}	6.69×10^{-13}	4.22×10^{-12}	1.08×10^{-12}	5.31×10^{-13}	8.39×10^{-14}	8.14×10^{-12}	5.49×10^{-26}	1.57×10^{-11}
320	3.68×10^{-20}	8.68×10^{-13}	6.01×10^{-13}	3.81×10^{-12}	9.94×10^{-13}	5.34×10^{-13}	9.48×10^{-14}	7.91×10^{-12}	3.24×10^{-25}	1.48×10^{-11}

[a]The overall rate coefficients (k_{total}) for the PSICl + OH radical reaction were calculated by adding the values for all the individual reaction pathways at the corresponding temperature.

https://doi.org/10.1021/acs.jpca.2c01203
J. Phys. Chem. A 2022, 126, 4264−4276

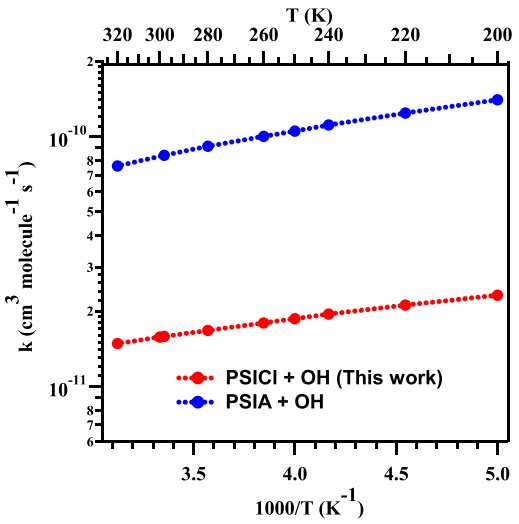

Figure 7. Comparison of the overall rate coefficients calculated for the PSICl + OH radical reaction with the available overall rate coefficients for the PSIA + OH radical reaction[44] in the temperatures between 200 and 320 K and a pressure of 1 atm.

mainly due to the presence of the −OH moiety in PSIA, which facilitates the labile H-atom abstraction by the OH radical, which in turn exhibits a very high negative barrier (approximately −4.7 kcal/mol) relative to the PSIA + OH radical separated reactants. This is not possible in the case of the PSICl + OH radical reaction. The results suggest that the OH radical-facilitated degradation of PSICl is slower than that of PSIA under atmospherically relevant conditions.

The rate coefficients for all the reaction paths were obtained by adding the tunneling contributions estimated using the Eckart tunneling[40] method in the studied temperature range. The obtained tunneling contributions for each of the H- and Cl-atom abstraction and substitution paths in the temperatures between 200 and 320 K are displayed in Table S10. The data indicate that the contribution due to tunneling for each reaction path decreases with increasing temperature, except for the substitution reaction path that proceeds via TS5, which is independent of tunneling in the studied temperature range. This observation is mainly because the imaginary frequency for this transition state is below 200 cm^{-1} (see Table S4).

The temperature and pressure dependent rate coefficients were calculated for the major reaction path (R5) associated with the PSICl + OH radical reaction to verify that the reaction occurs in the temperatures between 200 and 320 K. The bath gas pressures were varied between 0.1, 1.0, and 10 atm. The obtained rate coefficients at 0.1, 1.0, and 10 atm are given in Table S11. The data suggest that the rate coefficients for the major reaction channel are independent of pressure over the studied temperature range. For example, the rate coefficients at 298 K when the pressures were varied from 0.1, 1.0, and 10 atm were estimated to be 8.16×10^{-12}, 8.16×10^{-12}, and 8.20×10^{-12} cm^3 molecule^{-1} s^{-1}, respectively.

Branching ratios were calculated to reveal the relative contributions of each reaction path to the overall reaction for the PSICl + OH radical system in the studied temperature range. These are displayed in Table 3. The results suggest that the addition of the OH radical to the S-atom of the sulfinyl group followed by S(=O)−Cl single bond fission via TS5 leading to PSIA + Cl radical products contributes most to the overall reaction. The branching contribution from this pathway is ∼40.8% at 200 K and increases to ∼53.4% at 320 K. The next highest contributing reaction was found to be the abstraction of the H-atom by the OH radical via TS3a, with a branching ratio of ∼30.5% at 200 K, which decreased to 25.8% at 320 K. The branching ratio values in the present studied temperature range for the abstraction of the Cl-atom via TS1 were found to be $\sim 10^{12}$ to 10^{8} times smaller, and addition of the OH radical to the C-atom of the methylene group that proceeds via TS6 was found to be $\sim 10^{19}$ to 10^{13} times smaller when compared to the branching ratio values of the major reaction channel that occurs through TS5. The branching contributions for the other remaining H-atom abstraction reactions that proceed through TS2a, TS2b, TS3b, TS4a, and TS4b are ∼1−3 orders of magnitude smaller than the major reaction that occurs via TS5 (see Table 3).

4.2. Atmospheric Implications. The overall rate coefficients for the PSICl + OH radical reaction in the present studied temperatures between 200 and 320 K and with an average tropospheric concentration of [OH][68] = 1.0×10^6 molecules cm^{-3} were used in calculating the atmospheric lifetime of PSICl with respect to the OH radical in the same studied temperature range. The atmospheric lifetime (τ) of PSICl with the OH radical was computed using equation[69−71] $\tau = 1/(k_{overall}[OH])$. In this equation, $k_{overall}$ represents the overall rate coefficient for the PSICl + OH radical reaction and [OH] represents the average tropospheric concentration of the OH radical. Using the data obtained from the present work, the atmospheric lifetime of the PSICl with respect to OH radical was estimated to be ∼12−20 h in the temperatures between 200 and 320 K. This suggests that the atmospheric lifetime of PSICl with respect to its interaction with the OH radical in the atmosphere is ∼10 times larger than that of its parent molecule dipropyl thiosulfinate, whose lifetime in association with its reaction with

Table 3. Calculated Branching Ratios for All the Abstraction and Substitution Paths Involved in the PSICl + OH Radical Reaction in the Temperatures between 200 and 320 K and a Pressure of 1 atm

T	TS1	TS2a	TS2b	TS3a	TS3b	TS4a	TS4b	TS5	TS6
200	1.58×10^{-11}	9.3	6.7	30.5	9.3	3.2	0.21	40.8	1.27×10^{-18}
220	1.47×10^{-10}	8.4	5.9	30.3	8.5	3.1	0.25	43.4	2.21×10^{-17}
240	9.97×10^{-10}	7.7	5.3	29.7	8.0	3.1	0.30	45.9	3.55×10^{-16}
250	2.35×10^{-09}	7.3	5.1	29.3	7.7	3.1	0.33	47.1	1.31×10^{-15}
260	5.24×10^{-09}	7.0	4.9	28.9	7.5	3.1	0.36	48.1	4.55×10^{-15}
280	2.23×10^{-08}	6.6	4.5	27.9	7.2	3.2	0.44	50.1	4.50×10^{-14}
298	7.09×10^{-08}	6.2	4.3	27.0	6.9	3.4	0.52	51.7	2.88×10^{-13}
300	8.00×10^{-08}	6.2	4.3	26.9	6.9	3.4	0.53	51.9	3.50×10^{-13}
320	2.48×10^{-07}	5.9	4.1	25.8	6.7	3.6	0.64	53.4	2.19×10^{-12}

https://doi.org/10.1021/acs.jpca.2c01203
J. Phys. Chem. A 2022, 126, 4264−4276

the OH radical is reported to be ∼2 h.[20] Therefore, the atmospheric lifetime of PSICl with respect to the OH radical is very short (<1 day) in the present studied temperature range, and as such, its contribution to global warming is expected to be negligible. Nevertheless, its effect on global warming is anticipated to be ∼10 times higher than that of DPTS in terms of its reaction with the OH radical.

From the energetics, rate coefficients, and branching ratios, the dominant path is the formation of PSIA + Cl radical products from the reaction of the PSICl + OH radical. The most plausible degradation mechanism for the PSICl + OH radical reaction under atmospherically relevant conditions is proposed in Figure 8. As shown, the mechanism of the PSICl + OH radical reaction

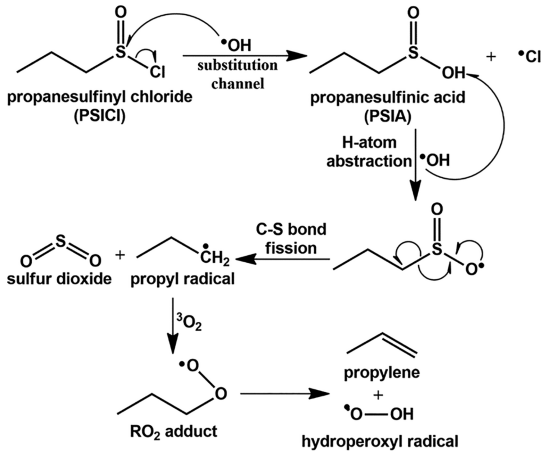

Figure 8. Proposed oxidation mechanism for the propanesulfinyl chloride + OH radical reaction under normal atmospheric conditions.

primarily proceeds through the substitution pathway (R5) to form PSIA + Cl radical products. The oxidation of PSIA with the OH radical was previously reported by our group.[44] The OH radical abstracts the H-atom from the −OH moiety of PSIA, leading to the formation of $CH_3CH_2CH_2S(=O)O^\bullet$ + H_2O as products.[44] Subsequent C−S single bond fission in the $CH_3CH_2CH_2S(=O)O^\bullet$ (as shown by the arrows) leads to the formation of sulfur dioxide (SO_2) and propyl radical products (see Figure 8).[44] Once formed, the propyl radical is expected to react with atmospheric oxygen ($^3O_2$) to form the corresponding RO_2 adduct (R = propyl radical). There are pathways available to this adduct which result in different outcomes. These include those involving internal rotation about the R−OO single bond, H-atom transfer reactions, reverse dissociation to form starting reactants, and direct elimination of the hydroperoxyl (HO_2) radical to form propylene. Based on the literature, it appears that the RO_2 radical adduct mainly proceeds to produce propylene + HO_2 radical products.[72]

The overall results reveal that, while PSICl itself makes a negligible contribution to global warming, the products of its relatively fast reaction with the OH radical fall under the category of long-lived greenhouse gases and pollutants such as SO_2, Cl radical, HO_2 radical, propylene, and water vapor, which have been shown to have major impacts on the formation of acid rain and SOA and contribute to global warming.

5. CONCLUSIONS

The OH radical initiated atmospheric oxidation mechanism and energetics of propanesulfinyl chloride have been studied for the first time using CCSD(T)//M06-2X and CCSD(T)//MP2 level calculations. The rate coefficients were calculated for all possible abstraction and substitution pathways using the Mesmer kinetic code in the temperatures between 200 and 320 K. The results indicate that, among all the possible reaction channels, the dominant one is the substitution path involving PSICl + OH radical reactants first forming a weakly bound PSICl··OH pre-reactive complex, which then undergoes isomerization through a transition state to form a PSIA··Cl post-reactive complex that leads to the formation of PSIA + Cl radical products. The computed branching ratios also showed this to be the major contributor to the overall reaction (i.e., ∼52%) at 298 K temperature and 1 atm pressure. The atmospheric lifetime of PSICl with respect to its reaction with the OH radical was calculated to be ∼12−20 h in the temperatures between 200 and 320 K. This result further supports the conclusion that this compound rapidly decomposes in the atmosphere, and as such, its effect on global warming will be negligible. However, the results also show that OH radical facilitated atmospheric degradation of PSICl produces SO_2, Cl radical, HO_2 radical, water, and propylene, each of which in its own right may contribute significantly to global warming, acid rain, and formation of secondary organic aerosols.

■ ASSOCIATED CONTENT

Supporting Information

The Supporting Information is available free of charge at https://pubs.acs.org/doi/10.1021/acs.jpca.2c01203.

(Tables S1−S11) The T1 diagnostic values, relative energies for various conformers, calculated total electronic energies including zero-point energy corrections calculated at various levels of theory, imaginary frequencies of various TSs at the M06-2X and MP2 levels, rotational constants at both the MP2 and M06-2X levels, optimized geometries of all the stationary points at both levels of theory, vibrational frequencies, tunneling contributions for all possible paths, and pressure-dependent rate coefficients for the major reaction channel; (Figure S1) conformers of propanesulfinyl chloride optimized at the M06-2X level (PDF)

■ AUTHOR INFORMATION

Corresponding Author

Rabi A. Musah − *Department of Chemistry, University at Albany—State University of New York, Albany, New York 12222, United States;* orcid.org/0000-0002-3135-4130; Email: rmusah@albany.edu

Author

Parandaman Arathala − *Department of Chemistry, University at Albany—State University of New York, Albany, New York 12222, United States;* orcid.org/0000-0002-9818-9686

Complete contact information is available at: https://pubs.acs.org/10.1021/acs.jpca.2c01203

Notes

The authors declare no competing financial interest.

■ ACKNOWLEDGMENTS

The financial support of the National Science Foundation (grant numbers 1310350 and 1710221) to R.A.M. is gratefully acknowledged. The authors thank the High-Performance

Computing Center at the University at Albany-SUNY for support.

REFERENCES

(1) Wine, P. H.; Thompson, R. J.; Semmes, D. H. Kinetics of OH reactions with aliphatic thiols. *Int. J. Chem. Kinet.* **1984**, *16*, 1623−1636.

(2) Charlson, R. J.; Lovelock, J. E.; Andreae, M. O.; Warren, S. G. Oceanic phytoplankton, atmospheric sulphur, cloud albedo and climate. *Nature* **1987**, *326*, 655−661.

(3) Boucher, O.; Moulin, C.; Belviso, S.; Aumont, O.; Bopp, L.; Cosme, E.; von Kuhlmann, R.; Lawrence, M. G.; Pham, M.; Reddy, M. S.; et al. DMS atmospheric concentrations and sulphate aerosol indirect radiative forcing: a sensitivity study to the DMS source representation and oxidation. *Atmos. Chem. Phys.* **2003**, *3*, 49−65.

(4) Graedel, T. E. Reduced sulfur emission from the open oceans. *Geophys. Res. Lett.* **1979**, *6*, 329−331.

(5) Montgomery, C. J.; Bockelie, M. J.; Sarofim, A. F.; Lee, J.; Bozzelli, J. W. "Thermochemical properties, reaction paths and kinetic mechanism for sulfur-chloro hydrocarbon combustion: Part I: thermochemistry and pyrolysis of chlorosulfides;" *American Flame Research Committee Internation Symposium on Combustion*; Livermore, CA, 2003.

(6) McFarland, B. L.; Boron, D. J.; Deever, W.; Meyer, J. A.; Johnson, A. R.; Atlas, R. M. Biocatalytic sulfur removal from fuels: applicability for producing low sulfur gasoline. *Crit. Rev. Microbiol.* **1998**, *24*, 99−147.

(7) Zhong, Q.; Shen, H.; Yun, X.; Chen, Y.; Ren, Y.; Xu, H.; Shen, G.; Du, W.; Meng, J.; Li, W.; Ma, J.; Tao, S. Global sulfur dioxide emissions and the driving forces. *Environ. Sci. Technol.* **2020**, *54*, 6508−6517.

(8) Kikuchi, R. Environmental management of sulfur trioxide emission: impact of SO_3 on human health. *Environ. Manag.* **2001**, *27*, 837−844.

(9) Finlayson-Pitts, B. J.; Pitts, J. J. N. *Chemistry of the Upper and Lower Atmosphere: Theory, Experiments, and Applications*; Academic Press: San Diego, United States, 2000.

(10) Hoesly, R. M.; Smith, S. J.; Feng, L.; Klimont, Z.; Janssens-Maenhout, G.; Pitkanen, T.; Seibert, J. J.; Vu, L.; Andres, R. J.; Bolt, R. M.; et al. Historical (1750−2014) anthropogenic emissions of reactive gases and aerosols from the community emissions data system (CEDS). *Geosci. Model Dev.* **2018**, *11*, 369−408.

(11) Kato, N.; Akimoto, H. Anthropogenic emissions of SO_2 and NO_x in Asia: emission inventories. *Atmos. Environ.* **1992**, *26*, 2997−3017.

(12) *Air Quality Guidelines for Europe*, 2nd ed.; World Health Organization, Ed.; WHO regional publications; World Health Organization, Regional Office for Europe: Copenhagen, 2000.

(13) Brimblecombe, P. *Air Composition and Chemistry*; Cambridge University Press: Cambridge, U.K., 1996.

(14) Lee, T.; Dirlam, P. T.; Njardarson, J. T.; Glass, R. S.; Pyun, J. Polymerizations with elemental sulfur: from petroleum refining to polymeric materials. *J. Am. Chem. Soc.* **2022**, *144*, 5−22.

(15) Puxbaum, H.; König, G. Observation of dipropenyldisulfide and other organic sulfur compounds in the atmosphere of a beech forest with *Allium ursinum* ground cover. *Atmos. Environ.* **1997**, *31*, 291−294.

(16) Oaks, D. M.; Hartmann, H.; Dimick, K. P. Analysis of sulfur compounds with electron capture/hydrogen flame dual channel gas chromatography. *Anal. Chem.* **1964**, *36*, 1560−1565.

(17) Block, E.; Putman, D.; Zhao, S. H. *Allium* chemistry: GC-MS analysis of thiosulfinates and related compounds from onion, leek, scallion, shallot, chive, and Chinese chive. *J. Agric. Food Chem.* **1992**, *40*, 2431−2438.

(18) Saito, K.; Horie, M.; Hoshino, Y.; Nose, N.; Mochizuki, E.; Nakazawa, H.; Fujita, M. Determination of allicin in garlic and commercial garlic products by gas chromatography with flame photometric detection. *J. Assoc. Off. Anal. Chem.* **2020**, *72*, 917−920.

(19) Arathala, P.; Musah, R. A. Theoretical studies of the gas-phase reactions of *S*-methyl methanesulfinothioate (dimethyl thiosulfinate) with OH and Cl radicals: reaction mechanisms, energetics, and kinetics. *J. Phys. Chem. A* **2019**, *123*, 8448−8459.

(20) Arathala, P.; Musah, R. A. Computational study investigating the atmospheric oxidation mechanism and kinetics of dipropyl thiosulfinate initiated by OH radicals and the fate of propanethiyl radical. *J. Phys. Chem. A* **2020**, *124*, 8292−8304.

(21) Arathala, P.; Musah, R. A. Oxidation of dipropyl thiosulfinate initiated by Cl radicals in the gas phase: implications for atmospheric chemistry. *ACS Earth Space Chem.* **2021**, *5*, 2878−2890.

(22) Thornton, J. A.; Kercher, J. P.; Riedel, T. P.; Wagner, N. L.; Cozic, J.; Holloway, J. S.; Dubé, W. P.; Wolfe, G. M.; Quinn, P. K.; Middlebrook, A. M.; et al. A large atomic chlorine source inferred from mid-continental reactive nitrogen chemistry. *Nature* **2010**, *464*, 271−274.

(23) Mielke, L. H.; Furgeson, A.; Osthoff, H. D. Observation of $ClNO_2$ in a mid-continental urban environment. *Environ. Sci. Technol.* **2011**, *45*, 8889−8896.

(24) Phillips, G. J.; Tang, M. J.; Thieser, J.; Brickwedde, B.; Schuster, G.; Bohn, B.; Lelieveld, J.; Crowley, J. N. Significant concentrations of nitryl chloride observed in rural continental Europe associated with the influence of sea salt chloride and anthropogenic emissions. *Geophys. Res. Lett.* **2012**, *39*, L10811.

(25) Bannan, T. J.; Booth, A. M.; Bacak, A.; Muller, J. B. A.; Leather, K. E.; Le Breton, M.; Jones, B.; Young, D.; Coe, H.; Allan, J.; et al. The first UK measurements of nitryl chloride using a chemical ionization mass spectrometer in central London in the summer of 2012, and an investigation of the role of Cl atom oxidation. *J. Geophys. Res.* **2015**, *120*, 5638−5657.

(26) Priestley, M.; le Breton, M.; Bannan, T. J.; Worrall, S. D.; Bacak, A.; Smedley, A. R. D.; Reyes-Villegas, E.; Mehra, A.; Allan, J.; Webb, A. R.; Shallcross, D. E.; Coe, H.; Percival, C. J. Observations of organic and inorganic chlorinated compounds and their contribution to chlorine radical concentrations in an urban environment in northern Europe during the wintertime. *Atmos. Chem. Phys.* **2018**, *18*, 13481−13493.

(27) Liu, X. X.; Qu, H.; Huey, L. G.; Wang, Y. H.; Sjostedt, S.; Zeng, L. M.; Lu, K. D.; Wu, Y. S.; Hu, M.; Shao, M.; Zhu, T.; Zhang, Y. High levels of daytime molecular chlorine and nitryl chloride at a rural site on the north china plain. *Environ. Sci. Technol.* **2017**, *51*, 9588−9595.

(28) Baker, A. K.; Sauvage, C.; Thorenz, U. R.; Van Velthoven, P.; Oram, D. E.; Zahn, A.; Brenninkmeijer, C. A.; Williams, J. Evidence for strong, widespread chlorine radical chemistry associated with pollution outflow from continental Asia. *Sci. Rep.* **2016**, *6*, 36821.

(29) Xie, H.-B.; Ma, F.; Wang, Y.; He, N.; Yu, Q.; Chen, J. Quantum chemical study on· Cl-initiated atmospheric degradation of monoethanolamine. *Environ. Sci. Technol.* **2015**, *49*, 13246−13255.

(30) Aneja, V. P.; Cooper, W. J. Biogenic Sulfur Emissions: a Review. *In Biogenic Sulfur in the Environment*; Saltzman, E. S.; Cooper, W. J., Eds.; ACS Symposium Series 393; American Chemical Society: Washington, DC, 1989; Chapter 1−13.

(31) Andreae, M. O.; Andreae, T. W. The cycle of biogenic sulfur compounds over the Amazon basin: 1. dry season. *J. Geophys. Res.* **1988**, *93*, 1487−1497.

(32) Haines, B.; Black, M.; Bayer, C. Sulfur Emissions from Roots of the Rain Forest Tree Stryphnodendron excelsum: Ecosystem, Community, and Physiological Implications. *Biogenic Sulfur in the Environment*; ACS Symposium Series; American Chemical Society, 1989; Vol. *393*, pp. 58−69.

(33) Faxon, C. B.; Allen, D. T. Chlorine chemistry in urban atmospheres: a review. *Environ. Chem.* **2013**, *10*, 221−233.

(34) Donaghy, T.; Shanahan, I.; Hande, M.; Fitzpatrick, S. Rate constants and atmospheric lifetimes for the reactions of OH radicals and Cl atoms with haloalkanes. *Int. J. Chem. Kinet.* **1993**, *25*, 273−284.

(35) Rowland, F. S. Stratospheric ozone depletion. *Philos. Trans. R. Soc., B* **2006**, *361*, 769−790.

(36) Crutzen, P. J. Albedo enhancement by stratospheric sulfur injections: a contribution to resolve a policy dilemma? *Clim. Change* **2006**, *77*, 211.

(37) Wigley, T. M. L. A combined mitigation/geoengineering approach to climate stabilization. *Science* **2006**, *314*, 452−454.

https://doi.org/10.1021/acs.jpca.2c01203
J. Phys. Chem. A 2022, 126, 4264−4276

(38) Robock, A.; Marquardt, A.; Kravitz, B.; Stenchikov, G. Benefits, risks, and costs of stratospheric geoengineering. *Geophys. Res. Lett.* **2009**, *36*, L19703.
(39) Glowacki, D. R.; Liang, C.-H.; Morley, C.; Pilling, M. J.; Robertson, S. H. MESMER: an open-source master equation solver for multi-energy well reactions. *J. Phys. Chem. A* **2012**, *116*, 9545−9560.
(40) Miller, W. H. Tunneling corrections to unimolecular rate constants, with application to formaldehyde. *J. Am. Chem. Soc.* **1979**, *101*, 6810−6814.
(41) Frisch, M. J.; Trucks, G. W.; Schlegel, H. B.; Scuseria, G. E.; Robb, M. A.; Cheeseman, J. R.; Scalmani, G.; Barone, V.; Petersson, G. A.; Nakatsuji, H.; et al. *Gaussian 16*, Revision B.01; Gaussian, Inc.: Wallingford, CT, 2016.
(42) Frisch, M. J.; Head-Gordon, M.; Pople, J. A. Semi-direct algorithms for the MP2 energy and gradient. *Chem. Phys. Lett.* **1990**, *166*, 281−289.
(43) Zhao, Y.; Truhlar, D. G. The M06 suite of density functionals for main group thermochemistry, thermochemical kinetics, noncovalent interactions, excited states, and transition elements: two new functionals and systematic testing of four M06-class functionals and 12 other functionals. *Theor. Chem. Acc.* **2008**, *120*, 215−241.
(44) Arathala, P.; Musah, R. A. Atmospheric oxidation of propanesulfinic acid initiated by OH radicals: reaction mechanism, energetics, rate coefficients, and atmospheric implications. *ACS Earth Space Chem.* **2021**, *5*, 1498−1510.
(45) Mai, T. V. T.; Nguyen, H. T.; Huynh, L. K. Kinetics of hydrogen abstraction from CH_3SH by OH radicals: An ab initio RRKM-based master equation study. *Atmos. Environ.* **2020**, *242*, 117833.
(46) Jørgensen, S.; Kjaergaard, H. G. Effect of hydration on the hydrogen abstraction reaction by HO in DMS and its oxidation products. *J. Phys. Chem. A* **2010**, *114*, 4857−4863.
(47) Zhao, Y.; Truhlar, D. G. Applications and validations of the Minnesota density functionals. *Chem. Phys. Lett.* **2011**, *502*, 1−13.
(48) Zhao, Y.; Truhlar, D. G. Density functionals with broad applicability in chemistry. *Acc. Chem. Res.* **2008**, *41*, 157−167.
(49) Kurtén, T.; Lane, J. R.; Jørgensen, S.; Kjaergaard, H. G. A computational study of the oxidation of SO_2 to SO_3 by gas-phase organic oxidants. *J. Phys. Chem. A* **2011**, *115*, 8669−8681.
(50) Wilson, A. K.; Dunning, T. H. The HSO−SOH isomers revisited: the effect of tight d functions. *J. Phys. Chem. A* **2004**, *108*, 3129−3133.
(51) Fukui, K. The path of chemical reactions - the IRC approach. *Acc. Chem. Res.* **1981**, *14*, 363−368.
(52) Arathala, P.; Tangtartharakul, C. B.; Sinha, A. Atmospheric ring-closure and dehydration reactions of 1,4-hydroxycarbonyls in the gas phase: the impact of catalysts. *J. Phys. Chem. A* **2021**, *125*, 5963−5975.
(53) Raghavachari, K.; Trucks, G. W.; Pople, J. A.; Head-Gordon, M. A fifth-order perturbation comparison of electron correlation theories. *Chem. Phys. Lett.* **1989**, *157*, 479−483.
(54) Noga, J.; Bartlett, R. J. The full CCSDT model for molecular electronic structure. *J. Chem. Phys.* **1987**, *86*, 7041−7050.
(55) Vereecken, L.; Francisco, J. S. Theoretical studies of atmospheric reaction mechanisms in the troposphere. *Chem. Soc. Rev.* **2012**, *41*, 6259−6293.
(56) Lee, T. J.; Taylor, P. R. A diagnostic for determining the quality of single-reference electron correlation methods. *Int. J. Quantum. Chem.* **1989**, *36*, 199−207.
(57) McKee, M. L. Computational study of addition and abstraction reactions between hydroxyl radical and dimethyl sulfide: a difficult case. *J. Phys. Chem.* **1993**, *97*, 10971−10976.
(58) Barone, S. B.; Turnipseed, A. A.; Ravishankara, A. R. Role of adducts in the atmospheric oxidation of dimethyl sulfide. *Faraday Discuss.* **1995**, *100*, 39−54.
(59) Wang, L.; Zhang, J. *Ab initio* study of reaction of dimethyl sulfoxide (DMSO) with OH radical. *Chem. Phys. Lett.* **2002**, *356*, 490−496.
(60) Parandaman, A.; Kumar, M.; Francisco, J. S.; Sinha, A. Organic acid formation from the atmospheric oxidation of gem diols: reaction mechanism, energetics, and rates. *J. Phys. Chem. A* **2018**, *122*, 6266−6276.
(61) Hyttinen, N.; Knap, H. C.; Rissanen, M. P.; Jørgensen, S.; Kjaergaard, H. G.; Kurtén, T. Unimolecular HO_2 loss from peroxy radicals formed in autoxidation is unlikely under atmospheric conditions. *J. Phys. Chem. A* **2016**, *120*, 3588−3595.
(62) Eskola, A. J.; Carr, S. A.; Shannon, R. J.; Wang, B.; Blitz, M. A.; Pilling, M. J.; Seakins, P. W.; Robertson, S. H. Analysis of the kinetics and yields of OH radical production from the $CH_3OCH_2 + O_2$ reaction in the temperature range 195−650 K: an experimental and computational study. *J. Phys. Chem. A* **2014**, *118*, 6773−6788.
(63) Piletic, I. R.; Edney, E. O.; Bartolotti, L. J. Barrierless reactions with loose transition states govern the yields and lifetimes of organic nitrates derived from isoprene. *J. Phys. Chem. A* **2017**, *121*, 8306−8321.
(64) Bartis, J. T.; Widom, B. Stochastic models of the interconversion of three or more chemical species. *J. Chem. Phys.* **1974**, *60*, 3474−3482.
(65) Urbanski, S. P.; Stickel, R. E.; Wine, P. H. Mechanistic and kinetic study of the gas-phase reaction of hydroxyl radical with dimethyl sulfoxide. *J. Phys. Chem. A* **1998**, *102*, 10522−10529.
(66) Bunkan, A. J. C.; Hetzler, J.; Mikoviny, T.; Wisthaler, A.; Nielsen, C. J.; Olzmann, M. The reactions of *N*-methylformamide and *N,N*-dimethylformamide with OH and their photo-oxidation under atmospheric conditions: experimental and theoretical studies. *Phys. Chem. Chem. Phys.* **2015**, *17*, 7046−7059.
(67) Jasper, A. W.; Miller, J. A. Lennard−Jones parameters for combustion and chemical kinetics modeling from full-dimensional intermolecular potentials. *Combust. Flame* **2014**, *161*, 101−110.
(68) Atkinson, R. Atmospheric chemistry of VOCs and NO_x. *Atmos. Environ.* **2000**, *34*, 2063−2101.
(69) Mishra, B. K.; Lily, M.; Deka, R. C.; Chandra, A. K. A theoretical insight into atmospheric chemistry of HFE-7100 and perfluoro-butyl formate: reactions with OH radicals and Cl atoms and the fate of alkoxy radicals. *New J. Chem.* **2016**, *40*, 6148−6155.
(70) Papadimitriou, V. C.; Kambanis, K. G.; Lazarou, Y. G.; Papagiannakopoulos, P. Kinetic study for the reactions of several hydrofluoroethers with chlorine atoms. *J. Phys. Chem. A* **2004**, *108*, 2666−2674.
(71) Kurylo, M. J.; Orkin, V. L. Determination of atmospheric lifetimes via the measurement of OH radical kinetics. *Chem. Rev.* **2003**, *103*, 5049−5076.
(72) Huang, H.; Merthe, D. J.; Zádor, J.; Jusinski, L. E.; Taatjes, C. A. New experiments and validated master-equation modeling for OH production in propyl+O_2 reactions. *Proc. Combust. Inst.* **2011**, *33*, 293−299.

https://doi.org/10.1021/acs.jpca.2c01203
J. Phys. Chem. A 2022, 126, 4264−4276